Supporting Information

Tailoring the Structure and Electrochemical Performance of Sodium Titanate Anodes by Post-synthesis Heating

Wei Yin,[a] Gözde Barim, [a] Xinxing Peng,[b],[c] Elyse A. Kedzie, [a], [d] Mary C. Scott,[b],[c] Bryan D. McCloskey,[a],[d] and Marca M. Doeff *[a]

[a] Energy Storage & Distributed Resources Division, Lawrence Berkeley National Laboratory, Berkeley, CA 94720, USA.
[b] Department of Materials Science and Engineering, University of California Berkeley, Berkeley, CA 94720, USA
[c] National Center for Electron Microscopy, Molecular Foundry, Lawrence Berkeley National Laboratory, Berkeley, CA 94720, USA
[d] Department of Chemical and Biomolecular Engineering, University of California Berkeley, Berkeley, CA, 94720, USA
* E-mail: mmdoeff@lbl.gov

Table of Contents

Experimental section

SI.1 Material Synthesis

Sodium titanate was synthesized *via* a two-step process involving solid state preparation of cesium titanate followed by ion-exchange.[1] First, cesium titanate $Cs_{0.74}Ti_{1.815}\square_{0.185}O_4$ was prepared by calcining under air a stoichiometric mixture of TiO_2 (99.8%, Sigma Aldrich) and Cs_2CO_3 (99.9%, Sigma-Aldrich) at 800 °C for 20 hours. The as-prepared $Cs_{0.74}Ti_{1.815}\square_{0.185}O_4$ was then converted to the sodium form by stirring the powder in 4 M NaCl aqueous solution at 80 °C in a heated mineral oil bath for 7 days. The resulting powder was then vacuum filtered, washed, and dried at 60 °C in an incubator. Heat treatment of sodium titanate powders was conducted under air at various temperatures for 8 h.

SI.2 Characterization

In situ synchrotron high-temperature XRD measurements on $Na_{0.74}Ti_{1.815}\square_{0.185}O_4 \cdot 1.27H_2O$ were performed at beamline 2–1 at the Stanford Synchrotron Radiation Lightsource (SSRL). Data was acquired in transmission mode using X-rays at 17 keV (λ = 0.729 Å) and a Pilatus 100K two-dimensional area detector with typical exposure times of 3 min. Powder samples were loaded into a 1.0 mm outer diameter quartz capillary that was subsequently loaded into a capillary heating sample cell described elsewhere.[2] Le Bail fitting of synchrotron XRD data were carried out using Fullprof Suite software to determine the unit cell parameters. Laboratory XRD data were collected on a Bruker D2 Phaser diffractometer with a CuKα source (λ = 1.5406 Å) equipped with a LynxEye detector. Raman spectroscopy and Fourier transform infrared-attenuated total reflection (FTIR-ATR) analyses were performed at the Molecular Foundry of Lawrence Berkeley National Lab (LBNL). Raman spectra were collected with a Horiba Labram Aramis confocal Raman microscope with 532 nm laser. FTIR-ATR spectra were collected with a PerkinElmer Spectrum One instrument equipped with horizontal attenuated total reflection assembly (HATR) on a ZnSe 45-degree plate. The morphology of the materials after heating at various temperatures were determined using a scanning electron microscope (SEM) (JEOL JSM-7500F). High-resolution transmission electron microscope (TEM) images were collected using a ThemIS operated at 300 kV at the National Center for Electron Microscopy of Lawrence Berkeley National Lab (LBNL). *Ex situ* Ti L-edge and O K-edge X-ray absorption near-edge structure (XANES) spectra were collected at beamline 10–1 of SSRL under ultrahigh vacuum (10^{-9} Torr) using the total electron yield (TEY) and fluorescence yield (FY) detectors. Soft XAS measurements were conducted with a 31-pole wiggler and a spherical grating monochromator with 20 mm entrance and exit slits, a 0.2 eV energy resolution and a 1 mm^2 beam spot. *Ex situ* Ti K-edge XANES spectra were collected in transmission modes at beamline 4-3 at SSRL. Calibration was applied to all spectra using the first inflection point of the corresponding Ti metal foil. *Ex situ* synchrotron X-ray diffraction data was collected on beamline 11-3 at SSRL. The X-ray wavelength was calibrated to be 0.9762 Å using a LaB_6 standard. All the *ex situ* samples were sandwiched between two layers of Kapton tape. Differential electrochemical mass spectrometry (DEMS) experiments allow the quantification of gas evolution during cell cycling. Note that the DEMS cells were rested at open circuit voltage (OCV) overnight to allow any chemical reactions (*e.g.*, electrolyte decomposition, reactions of adventitious water) and thereby the formation of a solid electrolyte interface (SEI) on the sodium metal surface. The cell headspace was then flushed with argon to remove the generated gases prior to start the galvanostatic cycling. More details about the setup and method can be found in prior publications.[3]

SI.3 Electrochemical Measurements

The composite electrodes were prepared by making a slurry of 70 *wt.*% sodium titanate, 20 *wt.*% acetylene black (Denka, 50 % compressed), 5 *wt.*% carboxymethyl cellulose (CMC) and 5 wt.% Styrene-Butadiene Rubber (SBR) in water solution. The slurry was then cast onto carbon-coated aluminum foil.

The electrodes were dried under vacuum at 60 °C or 100 °C for 12 hours before being punched into 1/2-inch disks in diameter. The typical electrode loadings and thicknesses were ~ 1.0 - 1.5 mg cm^{-2} and 150 μm, respectively. 2032-coin cells were assembled with metallic sodium foil (Sigma-Aldrich) as counter electrodes, GF/F glass fiber (Whatman) separators, and electrolyte solution of 0.5 M sodium tetraphenylborate ($NaBPh_4$, Sigma-Aldrich, as received) in diethylene glycol dimethyl ether (DEGDME, Anhydrous, Sigma-Aldrich, pre-dried with molecular sieve 3 Å). All the galvanostatic cycling measurements were performed using a VMP3 multichannel potentiostat/galvanostat (BioLogic) at a current rate of 8 mA g^{-1} (0.008 mA cm^{-2}).

Results and Discussion

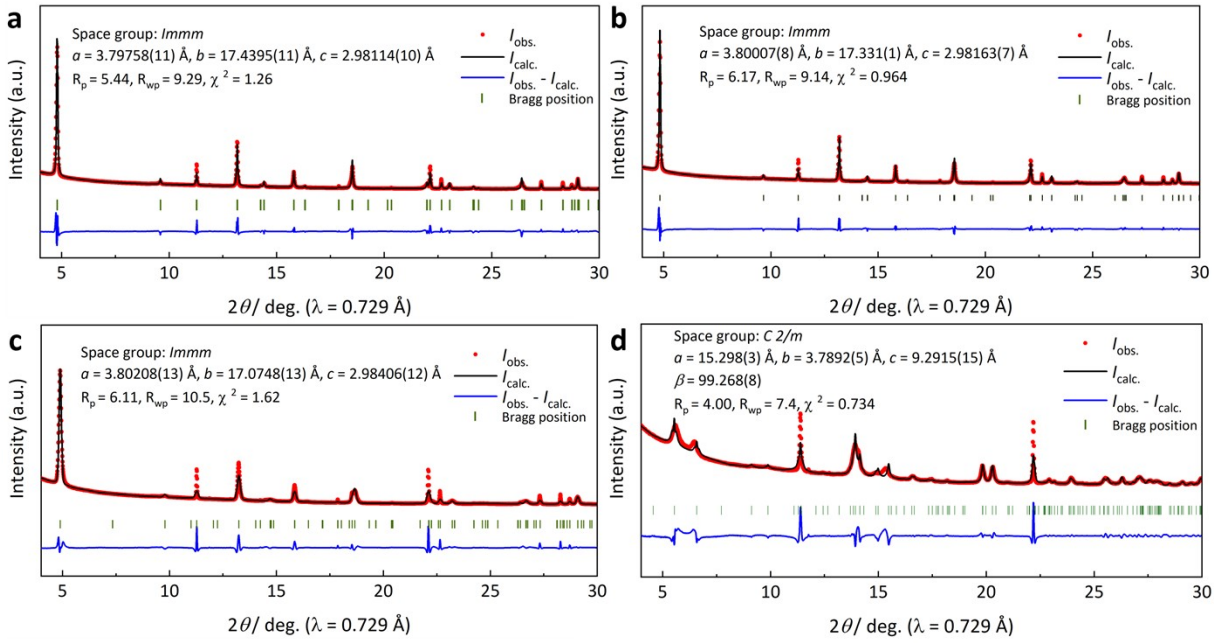

Figure S1 Le Bail fitting of XRD patterns of NTOs collected during the *in situ* high-temperature synchrotron XRD measurements at (a) 100 °C, (b) 125 °C, (c) 150 °C by adopting the *Immm* space group, and (d) 775 °C by adopting the *C2/m* space group.

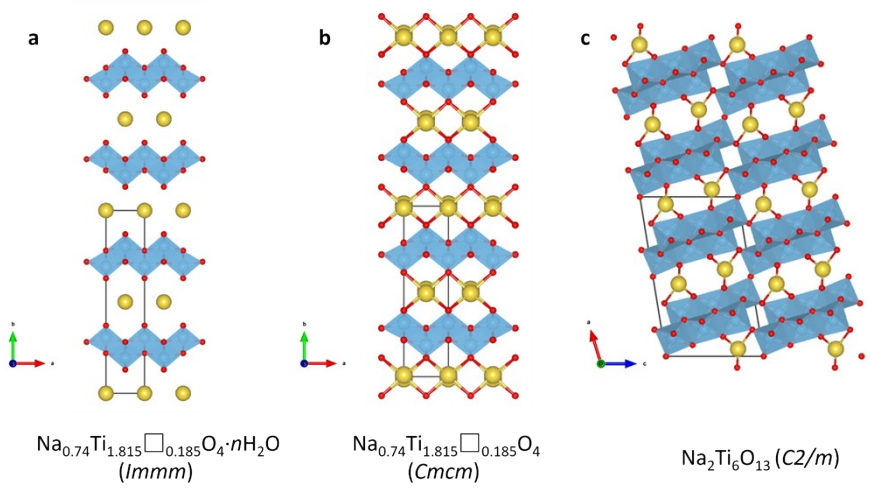

Figure S2 Schematic illustrations of crystal structures of (a) hydrous NTO ($Na_{0.74}Ti_{1.815}\square_{0.185}O_4{\cdot}nH_2O$), (b) anhydrous NTO ($Na_{0.74}Ti_{1.815}\square_{0.185}O_4$), and (c) $Na_2Ti_6O_{13}$. Gold spheres represent sodium atoms and blue polyhedra represent TiO_6.

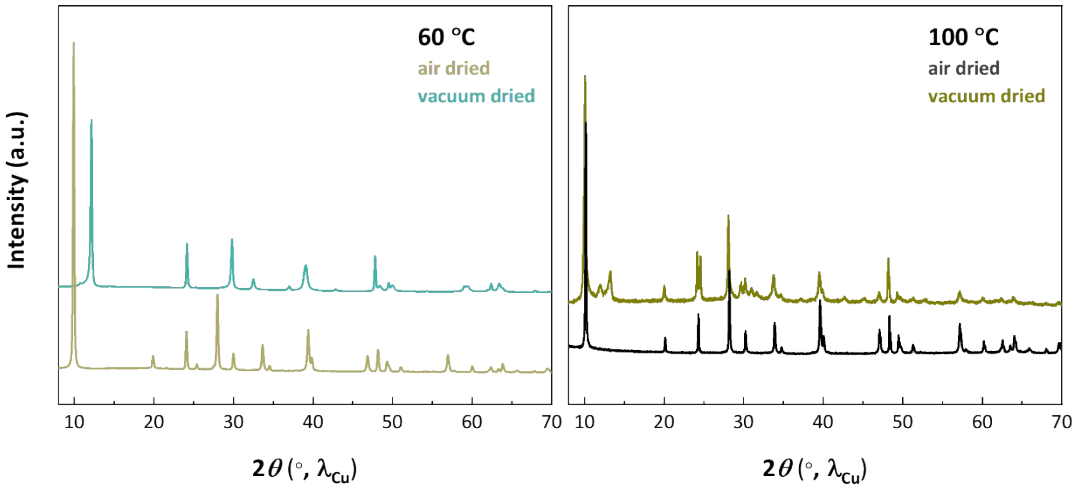

Figure S3 (a) *Ex situ* synchrotron XRD patterns for NTOs dried at 60°C and (b) *ex situ* laboratory XRD patterns for NTOs dried at 100°C under air and vacuum.

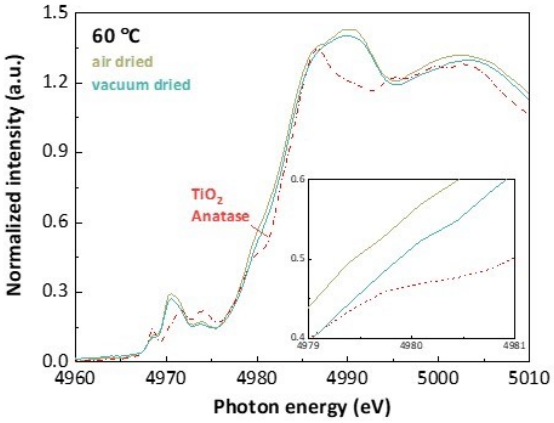

Figure S4 Ti K-edge X-ray absorption near-edge structure (XANES) spectra of NTOs heated at 60 °C under air and vacuum.

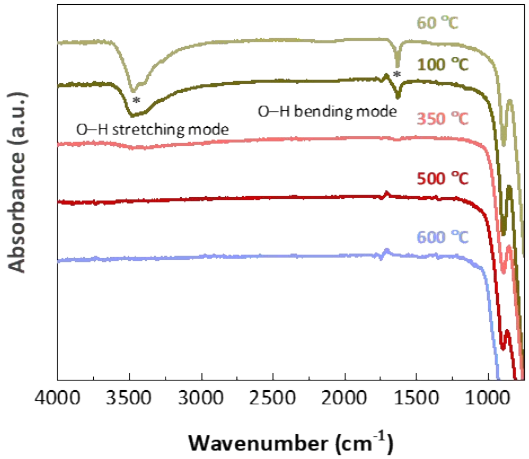

Figure S5 Fourier transform infrared spectroscopy (FTIR) spectrum collected for NTOs heated in air at various temperatures from 60 °C to 600 °C in attenuated total reflectance (ATR) mode.

The IR spectra of NTOs heated at lower temperatures of 60 °C and 100 °C showed a broad vibrational band centered at 3432 cm^{-1} along with a prominent peak at ca. 1634 cm^{-1}, which are typically assigned to the O−H stretching and bending modes of liquid water.[4, 5] These two IR vibrational bands become weaker in intensity as the heating temperature increased to 350 °C and were absent in the spectrum of 500 °C- and 600 °C heated NTO, due to the loss of physiosorbed water at elevated temperatures.

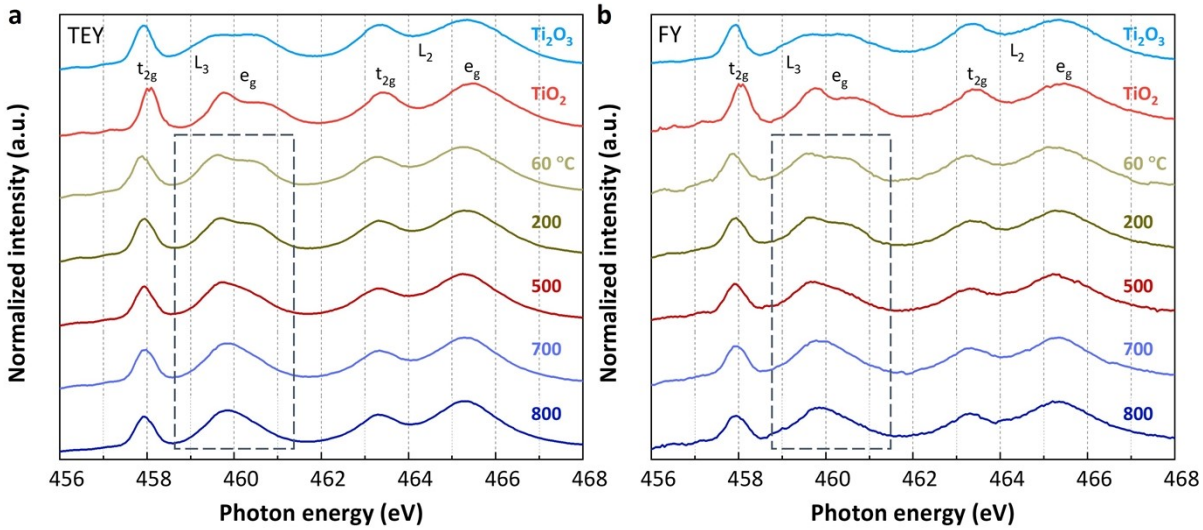

Figure S6 Ti L-edge X-ray absorption near-edge structure (XANES) spectra of NTOs heated in air at various temperatures from 60 °C to 800 °C collected in (a) total electron-yield (TEY) and (b) fluorescence-yield (FY) mode, respectively. References of Ti_2O_3 (cyan line) and anatase TiO_2 (red line) are included for comparison.

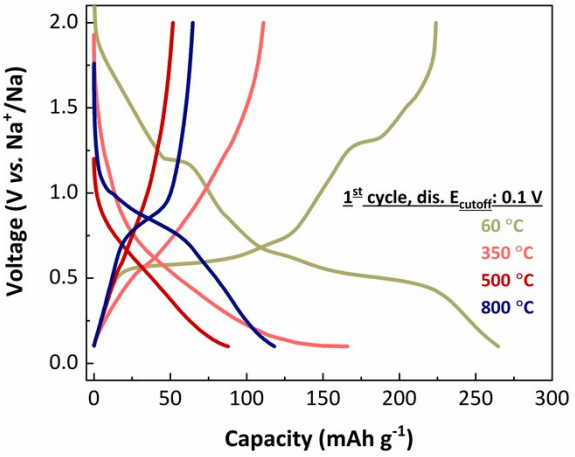

Figure S7 The first-cycle galvanostatic discharge-charge voltage profiles from 0.1 – 2.0 V *vs.* Na^+/Na of sodium half-cells containing NTOs heated at temperatures of 60, 350, 500, and 800 °C. All the cells were cycled at a current rate of 8 mA g^{-1} (0.008 mA cm^{-2}) and a solution of 0.5 M $NaBPh_4$ in DEGDME as the electrolyte.

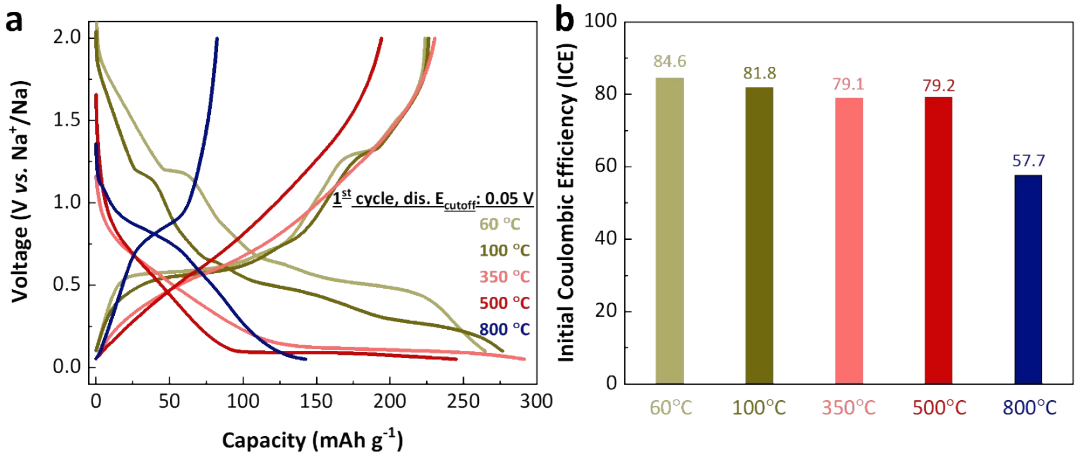

Figure S8 (a) The first-cycle galvanostatic discharge-charge voltage profiles and (b) initial coulombic efficiency (ICE) of cells containing NTOs heated at 60, 350, 500, and 800 °C. Cells made of 60 °C-heated NTO that were further vacuum dried at 100 °C were also included for comparison (denoted as '100 °C' in the figures). A cycling voltage window of 0.1 – 2.0 V *vs.* Na^+/Na was used for 60 °C- and 100 °C heated NTOs, whereas 0.05 – 2.0 V *vs.* Na^+/Na was used for 350 °C-, 500 °C-, and 800 °C heated NTOs. All the cells were cycled at a current rate of 8 mA g^{-1} (0.008 mA cm^{-2}) with sodium metal counter electrodes and a solution of 0.5 M $NaBPh_4$ in DEGDME as the electrolyte.

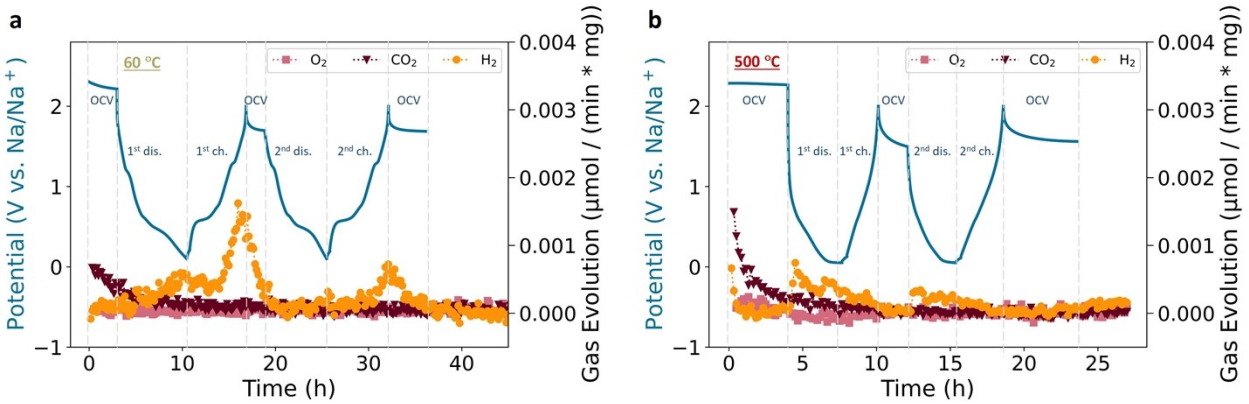

Figure S9 Gas evolution in the initial two cycles of sodium half cells made with (a) 60 °C- and (b) 500 °C heated NTOs. The cells were cycled at a current rate of 32 mA g^{-1} using 0.5 M $NaBPh_4$ in DEGDME as the electrolyte.

No other gas (molar mass ratio 1 – 80) besides H_2 was observed during cell cycling. The CO_2 signals observed during the open circuit voltage (OCV) period were from residual CO_2 in the instrument. H_2 generation could have multiple origins: i) reduction of physiosorbed and/or interlayer water from NTO electrodes, ii) chemical reactivity of water with sodium metal, and iii) reduction of protons that result from degradation of the salt or diglyme solvent. The H_2 evolution observed during charging in the cell with the 60 °C-heated NTO might be related to the formation of a fresh sodium metal surface caused by Na^+ stripping, which then further reacts with residual water in the cell. However, H_2 evolution was not detectable during the charge process of 500 °C-heated NTO cell because of its lower water content, suggesting that extraction of protons from the solvent was not a major contributor. This finding highlights the importance of proper dehydration in optimizing the electrochemical properties of NTO electrodes. Note that H_2 signals detected during the second OCV period is mostly from the residual H_2 generated during the previous charge.

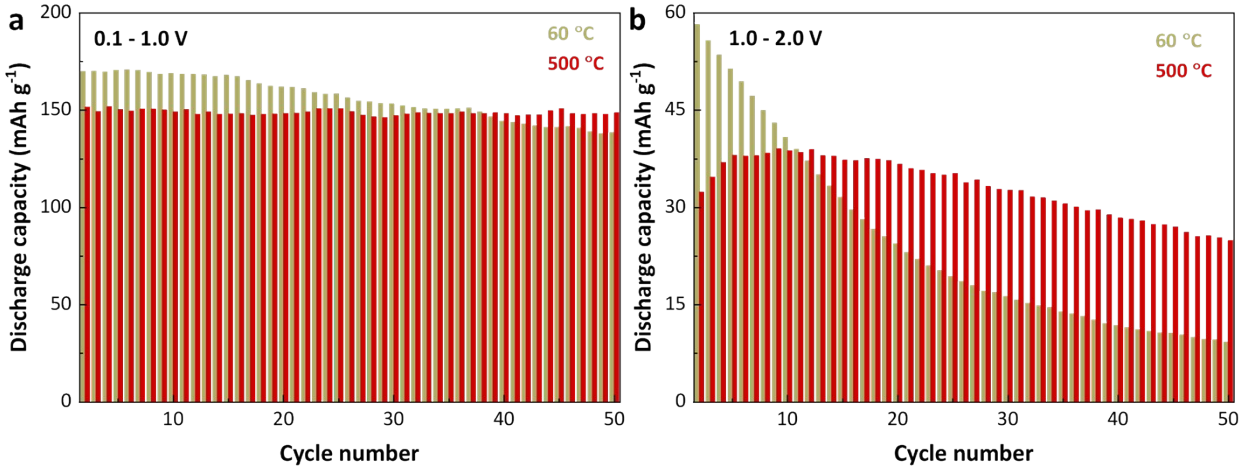

Figure S10 Capacity retention of cells containing 60 °C- and 500 °C heated NTOs in the voltage regions of (a) 0.1 – 1.0 V and (b) 1.0 – 2.0 V *vs.* Na^+/Na.

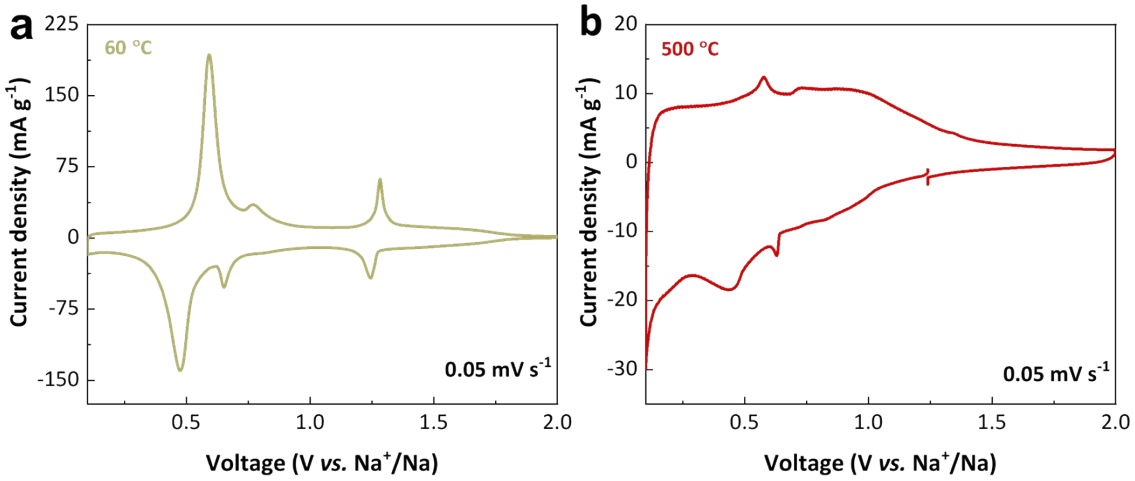

Figure S11 Cyclic voltammograms measured at 0.05 mV s^{-1} for (a) 60 °C- and (b) 500 °C heated NTOs.

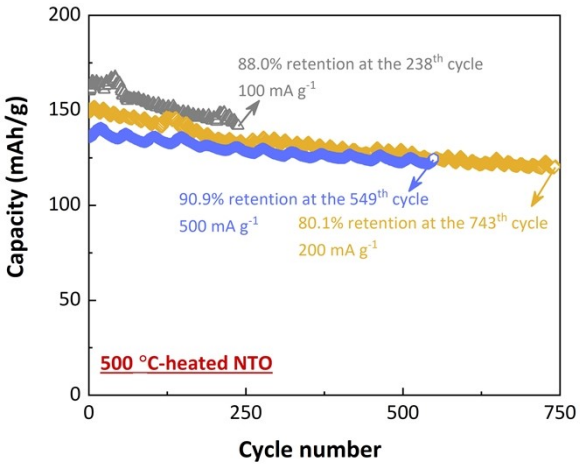

Figure S12 Capacity retention after two 'formation' cycles at 8 mA g^{-1} for sodium half cells containing 500 °C-heated NTO cycled at various current densities of 100, 200, and 500 mA g^{-1} using 0.5 M $NaBPh_4$ in DEGDME as the electrolyte. The periodic capacity fluctuations were due to temperature differences between day and night.

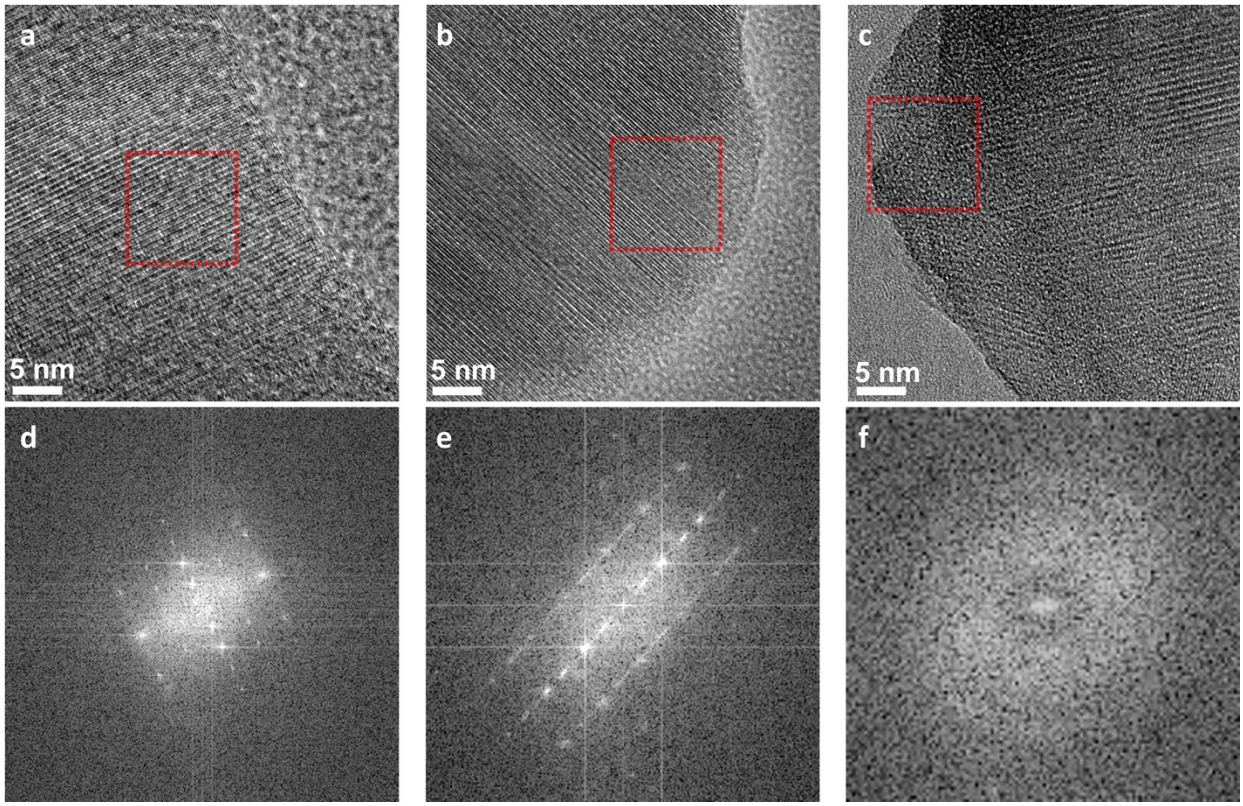

Figure S13 *Ex situ* HRTEM images of individual 500 °C-heated NTO particles in the (a) pristine state, and after initial discharge to (b) 0.1 and (c) 0.05 V *vs.* Na^+/Na. Their corresponding fast Fourier transform (FFT) patterns of the local regions highlighted by the red squares are shown in (d-f).

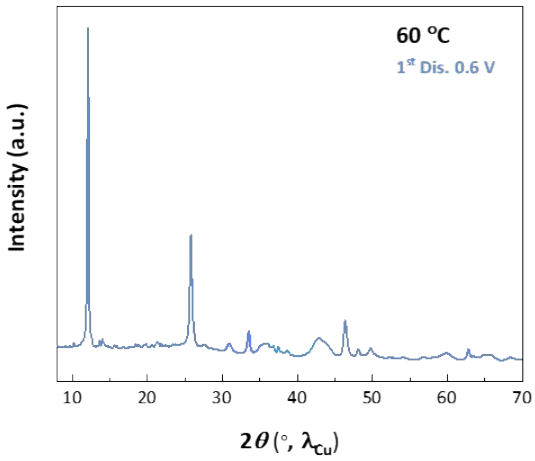

Figure S14 *Ex situ* synchrotron XRD pattern of 60 °C-heated NTO after initial discharge to 0.6 V *vs.* Na^+/Na.

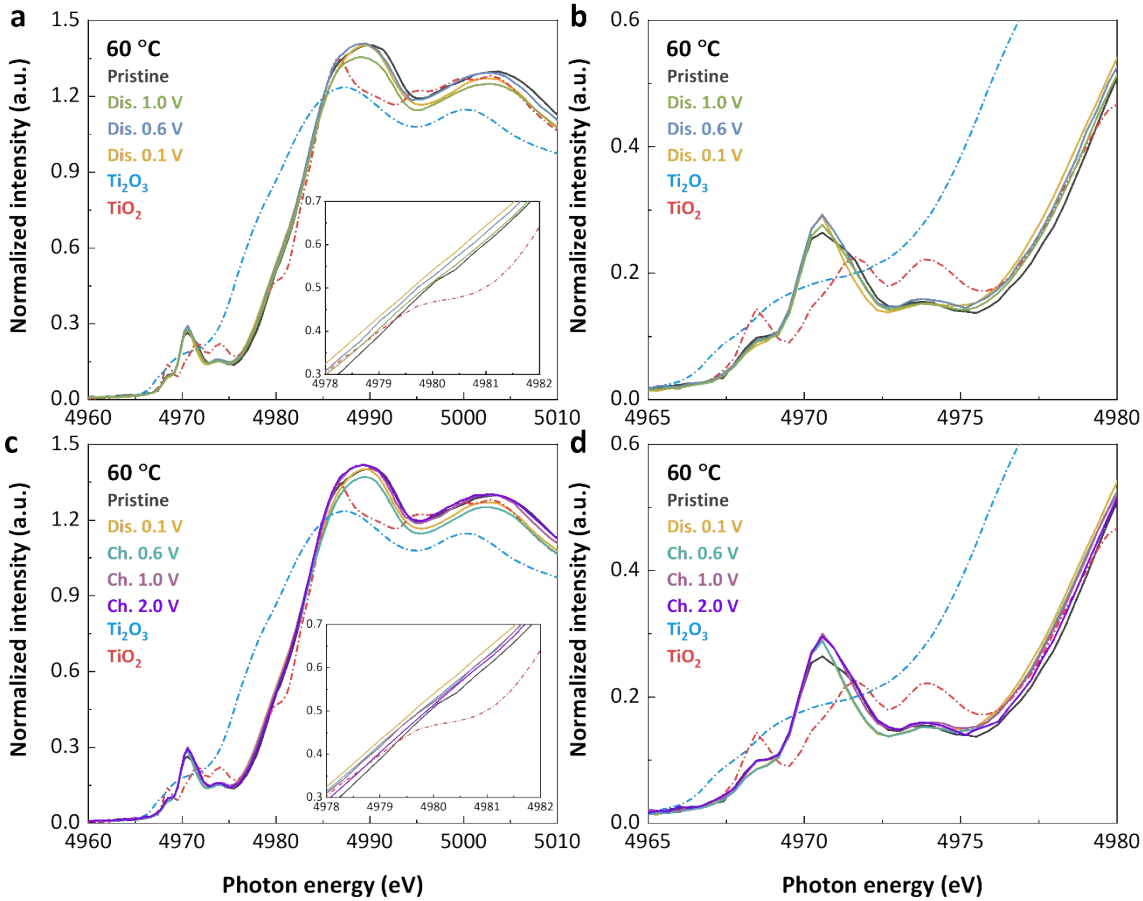

Figure S15 Ti K-edge X-ray absorption near-edge structure (XANES) spectra of 60 °C-heated NTO stopped at various points during (a) discharge and (c) charge in the first electrochemical cycle. Insets in (a) and (c) show the zoom-in of the edge region. (b) and (d) show the zoom-in of the pre-edge region.

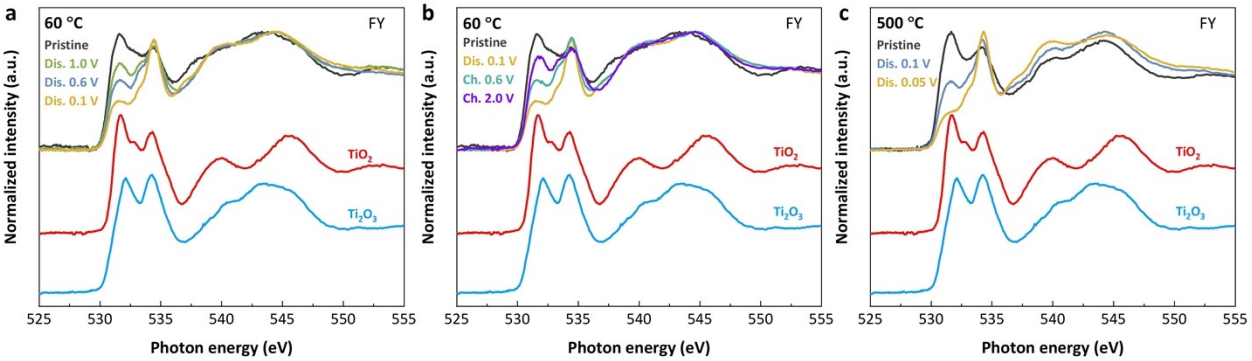

Figure S16 O K-edge X-ray absorption near-edge structure (XANES) spectra in the fluorescence yield (FY) mode for (a, b) 60 °C- and (c) 500 °C heated NTOs as a function of depth of discharge and charge in the initial electrochemical cycle.

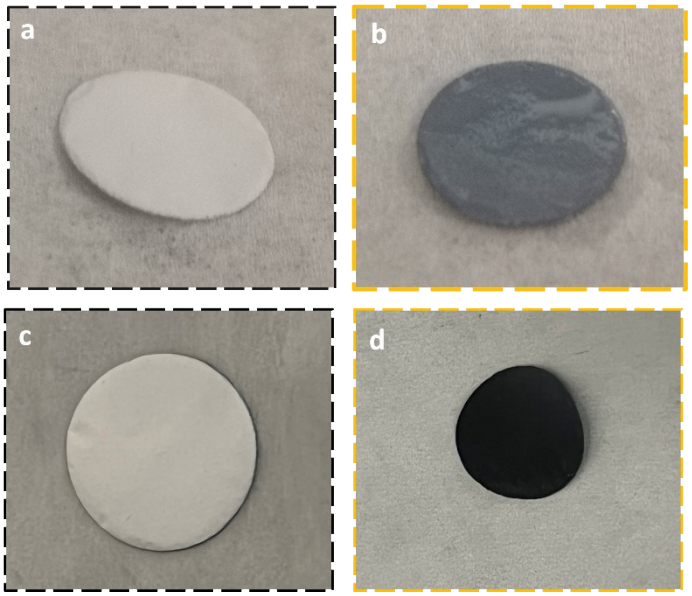

Figure S17 Optical images of carbon-free (a, b) 60 °C- and (c, d) 500 °C heated NTO electrodes in the (a, c) pristine and end-of-discharge states at (b) 0.1 and (d) 0.05 V *vs.* Na^+/Na.

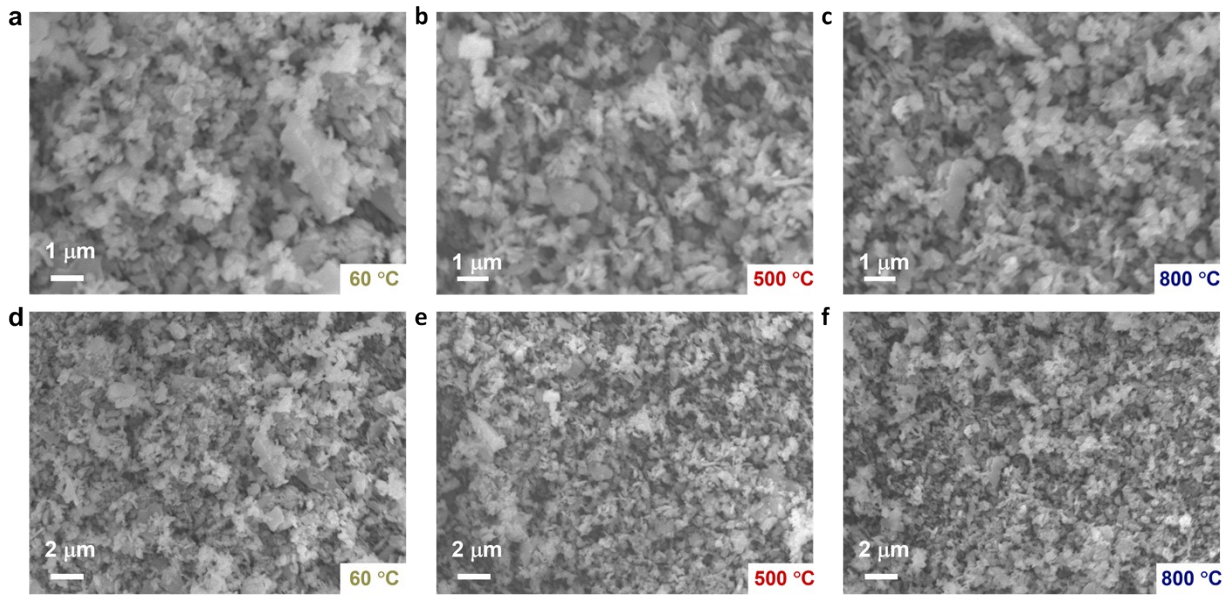

Figure S18 Scanning electron microscope (SEM) images of (a, d) 60 °C-, (b, e) 500 °C-, and (c, f) 800 °C-heated NTOs at various magnifications indicating no obvious change in the materials' morphology after heating at different temperatures.

References

1. W. Yin, J. Alvarado, G. Barim, M. C. Scott, X. Peng and M. M. Doeff, *MRS Energy & Sustainability*, 2021, DOI: 10.1557/s43581-021-00008-6.
2. A. S. Hoffman, J. A. Singh, S. F. Bent and S. R. Bare, *J Synchrotron Radiat*, 2018, **25**, 1673-1682.
3. B. D. McCloskey, D. S. Bethune, R. M. Shelby, G. Girishkumar and A. C. Luntz, *J Phys Chem Lett*, 2011, **2**, 1161-1166.
4. J. E. Bertie and Z. Lan, *Applied Spectroscopy*, 1996, **50**, 1047-1057.
5. A. A. Kananenka and J. L. Skinner, *J Chem Phys*, 2018, **148**, 244107.